# Creep-Induced Local Lattice Parameter Changes in a Monocrystalline Nickel-Base Superalloy

*H. Mughrabi, H. Biermann, and T. Ungár*

**The γ-γ′ lattice mismatch of specimens of the monocrystalline nickel-base superalloy SRR 99 has been measured by a high-resolution X-ray diffraction technique for the undeformed state and after high-temperature creep deformation. During creep deformation beyond the minimum creep rate (total strain ≈0.5%), the lattice mismatches, measured in and perpendicular to the [001] stress axis, respectively, undergo changes in opposite directions. This reflects the buildup of a complex deformation-induced triaxial state of internal stress in the phases γ and γ′. The overall resolved shear stresses that act in γ′ and γ due to the combined action of the external and internal stresses are estimated, and the conditions under which cutting of the γ′ phase by dislocations should occur are discussed.**

**Keywords**

high-temperature creep, internal stress, lattice mismatch, nickel-base superalloy, residual stress, X-ray diffraction

## 1. Introduction and Objectives

MONOCRYSTALLINE nickel-base superalloys with high γ′ volume fraction have become increasingly important as modern turbine blade materials. At high temperatures and under the action of an external or internal stress, the microstructure changes from cuboidal γ′ precipitates to a raft-like γ-γ′ structure.[1-4] Important factors that influence this microstructural change are the direction of external load and the sign and magnitude of the lattice mismatch, $\delta = 2(a_\gamma - a_{\gamma'})/(a_\gamma + a_{\gamma'})$, defined as the relative difference in the lattice parameters of the phases γ′ and γ, $a_{\gamma'}$ and $a_\gamma$ respectively. In the past, the γ-γ′ lattice mismatch has been investigated by different techniques.[5-11]

This article is a revised and up-dated version of a paper that was presented earlier.[12] The aim of the present work is to obtain reliable data about the local distribution of the lattice parameters of the phases γ and γ′ and the lattice mismatch, δ, of the monocrystalline nickel-base superalloy SRR 99 after high-temperature creep deformation. For this purpose, X-ray line profiles were measured with negligible instrumental line broadening and were evaluated to obtain the deformation-induced residual long-range internal stresses. From the superposition of the latter with the external stress, the resolved shear stresses acting in the slip systems of the type $\frac{1}{2}\langle 111\rangle\{101\}$ in the phases γ and γ′ are calculated and discussed with respect to the deformation behavior.

**H. Mughrabi** and **H. Biermann,** Institut für Werkstoffwissenschaften, Lehrstuhl I, Universität Erlangen-Nürnberg, D-91058 Erlangen, Federal Republic of Germany; and T. Ungár, Institute for General Physics, Eötvös University, H-1445 Budapest, P.O.B. 323, Hungary.

## 2. Experimental

### 2.1 *Samples*

Samples of the monocrystalline nickel-base superalloy SRR 99 with rod axes near [001] were investigated. In its initial state, the alloy is composed of a fcc γ matrix and of ordered $L1_2$ γ′ precipitates that are arranged in cubes of about 0.25 to 0.3 μm mean edge size with faces perpendicular to the <100> directions. The samples were standard heat treated by a single-stage annealing of 16 h at 870 °C. The γ′ volume fraction was determined as 71 ± 2% by analysis of X-ray line profiles of creep-deformed samples that were separated into γ and γ′ subprofiles, taking into account the different atomic scattering factors of the phases. This result was confirmed by complementary techniques.

The samples were creep deformed in tension at constant stresses, σ, between 150 and 750 MPa at temperatures of 750, 900, and 1050 °C.[13,14] The data from several specimens that were crept to rupture are given in Table 1.[13] All specimens were cooled to room temperature by an air blow to the grips immediately after fracture. One further set of samples was deformed at $T$ = 900 °C and σ = 305 MPa to different total strains (ε). Sample a was undeformed; samples b to e correspond to strains of 0.5, 1.5, 3.0, and 21.3%, respectively.[13] In all samples creep deformed until rupture at 1050 °C and in the samples deformed at 900 °C under stresses of 305 and 444 MPa, a raft-like γ-γ′ structure developed. The other samples still had a cuboidal γ′ structure even at the end of creep deformation.

### 2.2 *X-Ray Diffraction Technique*

From the creep-deformed specimens, {001}-oriented slices were cut by spark erosion and polished. One type of specimen was cut perpendicular to the [001] direction of the stress axis and investigated with the (002) Bragg reflection (axial case). The other type of specimen was perpendicular to the [010] (equivalent to [100]) direction and was studied with the (020)/(200) Bragg reflection (side case). The X-ray line profiles were measured with monochromatic $Cu_{K\alpha}$ radiation, using a special double-crystal diffractometer with high angular resolution and negligible instrumental line broadening.[10,11]

**Table 1 Data from creep tests**[13]

| Sample No. | $T$, °C | σ, MPa | $E$, GPa | $\varepsilon_f$, % | $t_f$, h | $\dot{\varepsilon}_{ss}$, $s^{-1}$ |
|---|---|---|---|---|---|---|
| 1 | 1050 | 150 | 86.0 | 13.2 | 133.6 | $3.0 \times 10^{-7}$ |
| 2 | 1050 | 200 | 86.0 | 19.4 | 31.9 | $1.2 \times 10^{-6}$ |
| 3 | 1050 | 305 | 84.9 | 25.0 | 2.8 | $3.0 \times 10^{-5}$ |
| 4 | 900 | 305 | 98.1 | 21.3 | 515.5 | $1.2 \times 10^{-7}$ |
| 5 | 900 | 444 | 104.5 | 28.7 | 89.3 | $7.0 \times 10^{-7}$ |
| 6 | 900 | 444 | 98.0 | 30.0 | 83.2 | $7.1 \times 10^{-7}$ |
| 7 | 900 | 607 | 96.6 | 24.2 | 6.7 | $6.8 \times 10^{-6}$ |
| 8 | 900 | 607 | 97.5 | 25.1 | 10.0 | $6.5 \times 10^{-6}$ |
| 9 | 900 | 750 | 98.5 | 24.4 | 0.7 | $7.0 \times 10^{-5}$ |
| 10 | 750 | 750 | 109.6 | 22.4 | 1348.3 | $2.8 \times 10^{-8}$ |
| 11* | 750 | 750 | 109.6 | 19.7 | 400.8 | $1.3 \times 10^{-7}$ |

**Note:** The values of Young's modulus, $E$, were calculated for the slightly differing orientations using the appropriate high-temperature elastic constants that had been reported by Kuhn and Sockel[16] for an alloy similar to SRR 99. $\varepsilon_f$, strain to failure; $t_f$, time to failure; $\dot{\varepsilon}_{ss}$, quasi-steady-state creep rate.
* This sample has been predeformed in tensile creep at $T$ = 900 °C, σ = 305 MPa, to a strain of 3% and annealed for 10 min at 1080 °C to obtain a raft structure prior to the creep test.

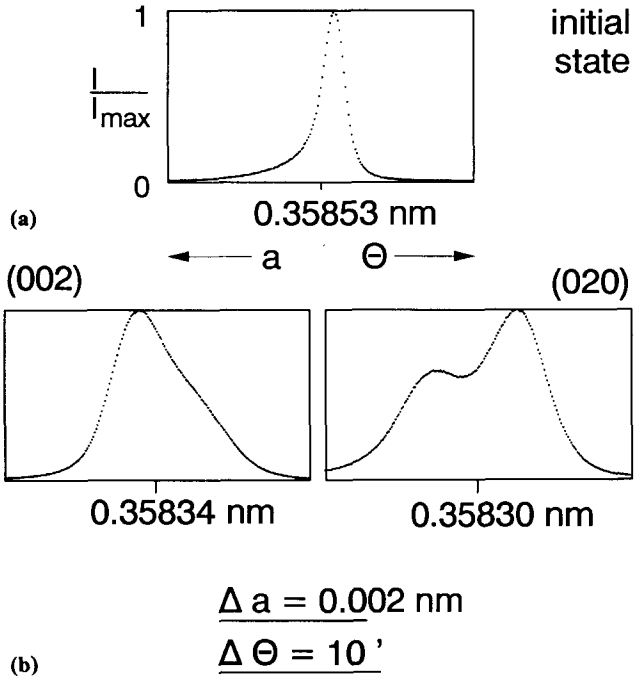


**Fig. 1** X-ray line profiles. (a) Undeformed state. (b) (002) and (020) Bragg reflections of the creep-deformed sample 3 (σ = 305 MPa at $T$ = 1050 °C).[11] The stated lattice parameters refer to the centers of gravity of the profiles.

The specimens were rotated continuously around the exact Bragg angle to probe the exact lattice parameter distribution of the sample.[10] The fact that the line profiles were not broadened due to instrumental effects was confirmed by the observation that the line profiles of type {002} and {004} had identical shapes. The absolute Bragg angles (and lattice parameters) were evaluated using a high-purity nickel single crystal as a reference. The reported values were calculated as a mean value from at least four line profiles.

## 3. Results

### 3.1 *Samples Creep-Deformed at 1050 °C*

First, a short review of earlier results obtained on samples that were creep deformed at 1050 °C[10,11] is given to compare these data with results of creep deformation at different temperatures. Figure 1 shows typical line profiles of alloy SRR 99 in the initial standard heat treated state (Fig. 1a) and after creep deformation and cooling to room temperature (Fig. 1b). The (002) line profile of the undeformed sample, which is indistinguishable from the (200) and (020) profiles, shows a pronounced asymmetry on the left side. This is due to the smaller volume fraction and the larger lattice parameter of the γ phase (i.e., negative constrained lattice mismatch in the undeformed state, $\delta_{undef} = -1.4 \times 10^{-3}$).[10] Hence, the maximum of the profile can be assigned primarily to the γ′ phase and the more slowly decreasing tail on the lower angle side to the γ phase.

The X-ray line profiles of a sample creep deformed at a constant stress of 305 MPa are shown in Fig. 1(b).[11] These profiles are broadened markedly in comparison to those of the undeformed sample and exhibit dramatically changed shapes. In the axial case, the profile has a reversed asymmetry on the right side and even exhibits a shoulder, whereas the (020) line profile (side case) shows the original asymmetry, which has however become more pronounced, as evidenced by the appearance of a second peak. The shape of line profiles of samples deformed at stresses of 150 and 200 MPa are intermediate between those shown in Fig. 1(a) and (b).

The profiles of the deformed samples can be separated by a mirror procedure,[10] which yields the subprofiles of the γ and γ′ phases. The result of this evaluation is that the centers of gravity of the subprofiles are shifted apart from each other in the side case, whereas they are shifted toward each other and even overlap in the axial case.

As shown in Fig. 2(a), the lattice parameter of γ′ in the [010] direction, $a^{\gamma}_{[010]}$, decreases with the applied stress, whereas the lattice parameter in the [001] direction, $a^{\gamma}_{[001]}$, increases. The strongest change in the lattice parameter is found for the γ phase

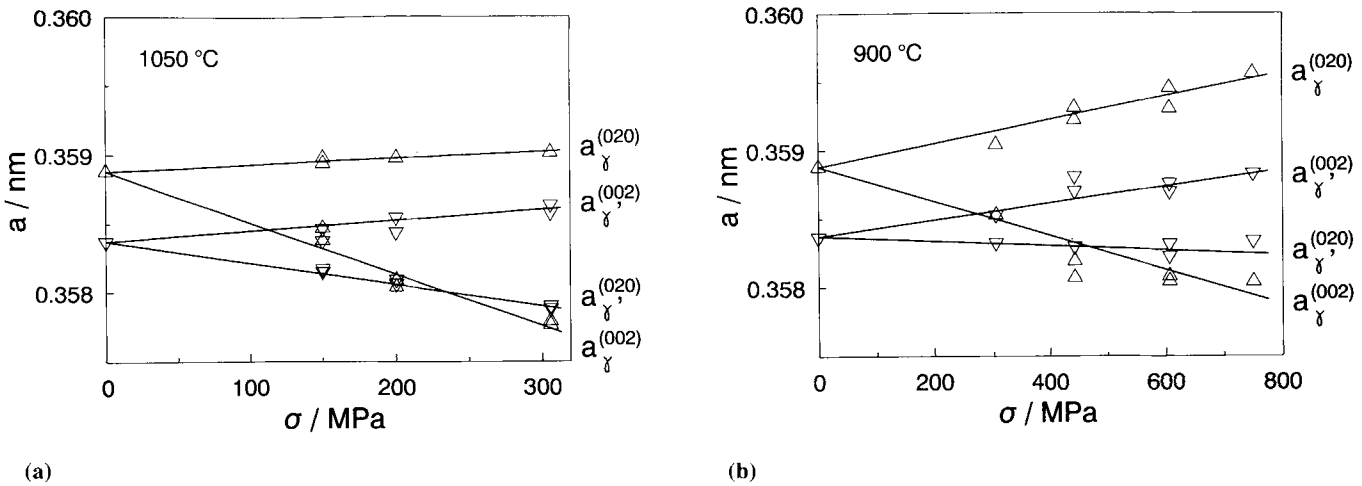


**Fig. 2** Lattice parameters of γ and γ′ versus applied stress for the (002) and (020) planes. (a) Samples 1 to 3, $T = 1050$ °C.[11] (b) Samples 4 to 9, $T = 900$ °C.

in the direction of the applied stress; $a^{\gamma}_{[001]}$ decreases by about 0.3%. On the other hand, $a^{\gamma}_{[010]}$ exhibits only a small increase. It is evident that the mean lattice parameters evaluated from the centers of gravity of the line profiles decrease with increasing applied stress.

### 3.2 *Samples Creep Deformed at 900 °C*

#### 3.2.1 Creep Deformation to Rupture at Different Stresses

The change in the line profiles of samples creep deformed at 900 °C (samples 4 to 9) with increasing applied stress is similar to that of samples deformed at the higher temperature. The profiles are, however, broadened more markedly and therefore more difficult to separate than the profiles of samples 1 to 3. The dependence of the lattice parameters as a function of the applied stress is illustrated in Fig. 2(b), which shows that $a^{\gamma}_{[001]}$ decreases considerably, but not as strongly as after creep at 1050 °C. The values of $a^{\gamma}_{[001]}$ increase, the increase being slightly stronger than that shown in Fig. 2(a) for samples creep deformed at 1050 °C. The (002) profile (axial case) of the sample deformed at 305 MPa is nearly symmetrical. Therefore, the stated lattice parameter represents the mean value obtained from the center of gravity of the corresponding line profile. The lines represent a best fit to each set of data points. The (002) measurements for $\sigma = 444$ MPa were not included in these fits, because the only very slight asymmetry in the line profiles led to some uncertainty in the peak separation procedure. The (002) profiles of samples deformed at 607 and 750 MPa are asymmetric, but due to their broadening they do not exhibit separate shoulders like sample 3 in Fig. 1(b). The (020) line profiles (side case), however, always exhibited a separate shoulder, and the lattice parameter values obtained have a smaller error than those of the (002) profiles. In the axial case, the lattice parameters of the γ phase increase strongly compared to the 1050 °C data. The $a^{\gamma}_{[001]}$ values decrease with increasing applied stress.

#### 3.2.2 Creep Deformation at $\sigma = 305$ MPa to Different Strains

Figure 3(a) shows the differentiated creep curve in a semilogarithmic plot with a minimum creep rate at $\varepsilon \approx 0.5\%$ and a quasi-steady-state (ss) regime beyond $\varepsilon \approx 3\%$. Sample a represents the undeformed state; sample b was unloaded at the minimum creep rate. Samples c and d correspond to the strains at which raft formation begins and is completed, respectively. Sample e (identical to sample 4) was deformed to rupture.

The line profiles of sample b are indistinguishable from profiles of undeformed samples. At a strain of 1.5% (sample c), the (002) profiles are symmetrical, and the (020) profiles exhibit a separate shoulder on the lower angle side (Fig. 3b). The profiles of samples c to e do not differ significantly from one another.

### 3.3 *Samples Creep Deformed at 750 °C*

The two samples investigated at this temperature were deformed at a stress of $\sigma = 750$ MPa. One sample had a cuboidal γ′ microstructure (sample 10) and one a prerafted microstructure (sample 11). The creep rate of the prerafted sample was found to be about one order of magnitude larger than that of the sample with the cuboidal γ-γ′ microstructure. The (002) line profiles of sample 10 exhibit an asymmetry on the higher angle side and the (020) line profiles a small asymmetry on the lower angle side. The shape of the line profiles of prerafted sample 11 is very different from that of sample 10. The (002) line profile has a second peak on the higher angle side, whereas the (020) profile is broadened markedly and nearly symmetrical. This (020) line profile can be separated into two subprofiles corresponding to the phases γ and γ′. The γ subprofile is situated on the lower angle side relative to the γ′ subprofile. The sense of the asymmetries of the two samples corresponds to that of samples 1 to 9. However, the magnitude of the shift of the subprofiles differs noticeably from that of the other samples.

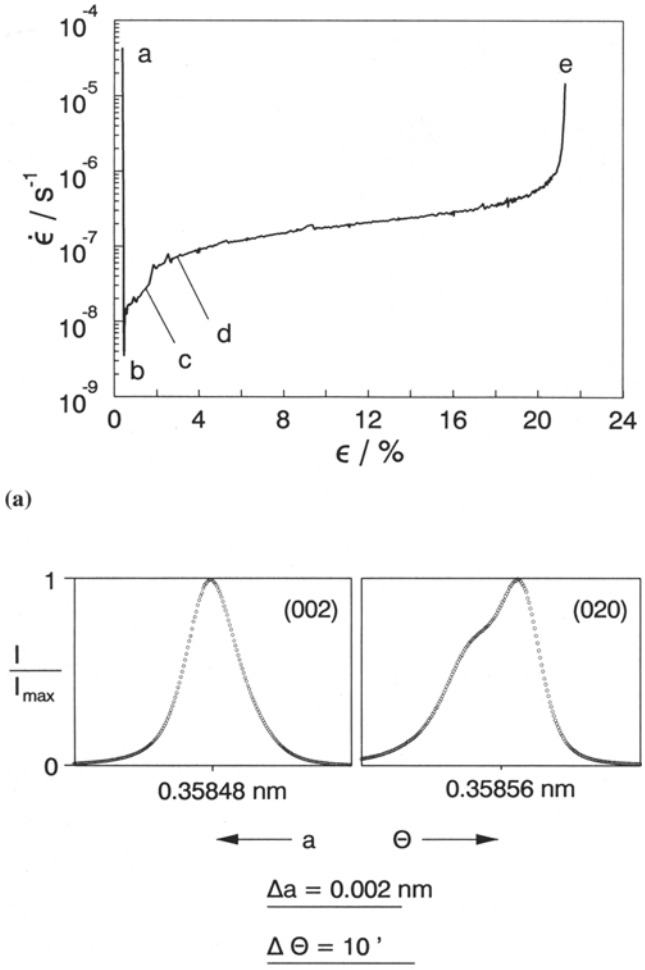


**Fig. 3** (a) Creep rate versus strain of samples b to e deformed to different strains ε at σ = 305 MPa and $T$ = 900 °C.[13] (b) X-ray line profiles of sample e (ε = 21.3%), which is identical to Sample 4 (Table 1).

## 4. Discussion

### 4.1 γ-γ′ *Lattice Mismatch*

#### 4.1.1 Mismatch as a Function of Stress

In Fig. 4(a) and (b), the values of the so-called constrained lattice mismatch, δ, of samples deformed at 1050 and 900 °C, measured at room temperature, are given as a function of applied stress. The mismatch of the undeformed state, $\delta_{undef} = -1.4 \times 10^{-3}$, was not evaluated from the line profiles, but from so-called ω-2θ scans of the intensity distribution in reciprocal space.[10] The γ-γ′ lattice mismatch values of deformed samples were determined as $\delta_{[001]}$ and $\delta_{[010]}$ for the Bragg reflections (002) and (020) in the directions [001] and [010], respectively. Their dependence on the applied stress is shown in Fig. 4. The γ-γ′ mismatch shows a strong dependence on applied stress for the {002} lattice planes both parallel and perpendicular to the external stress axis. The mismatch of the side case in the [010] direction, δ[010], decreases slowly with increasing external stress; δ[001] increases very strongly to $\delta[001] \approx +2.4 \times 10^{-3}$ ($T$ = 1050 °C and σ = 305 MPa) and to $\delta_{[001]} \approx +2.2 \times 10^{-3}$ ($T$ = 900 °C and σ = 750 MPa). The values of $\delta_{[001]}$ for $T$ = 1050 °C, σ = 150 MPa (sample 1) and $T$ = 900 °C, and σ = 305 MPa (sample 4) and 444 MPa (samples 5 and 6) cannot be given, because the profiles were either symmetrical (samples 1 and 4), or had only a small asymmetry (samples 5 and 6) and were therefore not separable. It is clear, however, that δ[001] should be near zero for $T$ = 1050 °C, σ = 150 MPa and $T$ = 900 °C, σ = 350 MPa, in accordance with the dependence shown in Fig. 2. For the following evaluations, δ[001] = 0 will be taken as an approximation in these cases. In the case of samples 5 and 6, δ[001] is determined by interpolation to be $0.9 \times 10^{-3}$. The corresponding mismatch values of samples 10 and 11 ($T$ = 750 °C, σ = 750 MPa) were found to be $\delta_{[001]} = +2.4 \times 10^{-3}$ and $+4.9 \times 10^{-3}$ and $\delta_{[010]} = -1.8 \times 10^{-3}$ and $-3.3 \times 10^{-3}$, respectively.

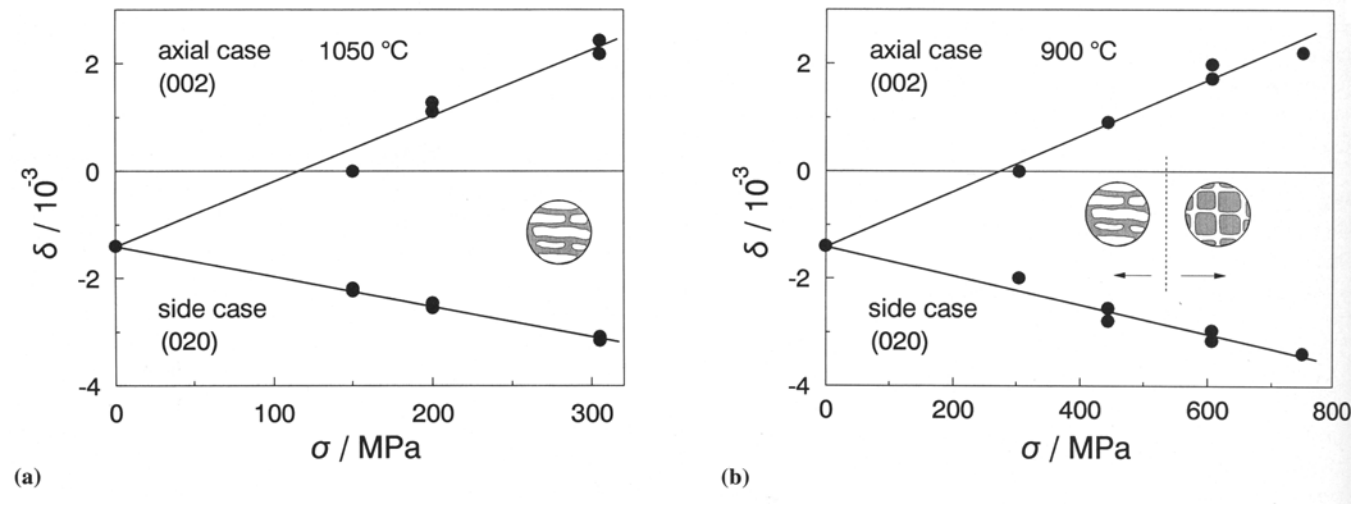


**Fig. 4** γ-γ′ lattice mismatch versus applied stress for (a) 1050 °C[11] and (b) 900 °C. The circular inserts in the figures represent the γ-γ′ microstructure after fracture of samples without predeformation.

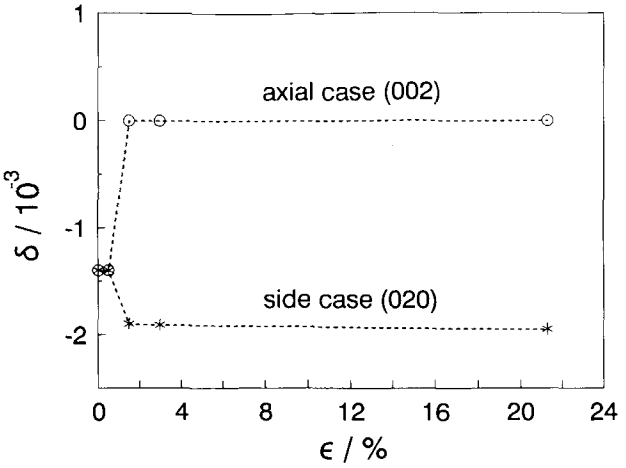


**Fig. 5** $\gamma$-$\gamma'$ lattice mismatch of samples deformed at 900 °C and 305 MPa to different strains (see Fig. 3).

### 4.1.2 Mismatch as a Function of Strain

In Fig. 5, the constrained lattice mismatch values, $\delta$, are plotted for the specimens that were creep deformed at 900 °C and at a stress of 305 MPa to different strains (Fig. 3a). The lattice mismatches, $\delta_{[001]}$ and $\delta_{[010]}$, of sample b, which was deformed to $\varepsilon = 0.5\%$, are both equal to $-1.4 \times 10^{-3}$ of the deformed state. The (002) line profiles (axial case) of samples c to e are almost symmetrical and therefore not separable, the mismatch is about zero. In the side case, the lattice mismatches are $-1.90 \times 10^{-3}$, $-1.91 \times 10^{-3}$, and $-1.95 \times 10^{-3}$ for the strains of 1.5, 3, and 21.3%, respectively. These mismatch values are, within the scatter due to separation of the line profiles, constant in the range of strains from $\varepsilon = 1.5\%$ until rupture ($\varepsilon = 21.3\%$).

### 4.2 *Deformation-Induced Residual Long-Range Internal Stresses*

The shifts of the subprofiles and the change of the lattice parameters of the $\gamma$ and $\gamma'$ phases can be described in terms of residual long-range internal stresses, as explained by a composite model.[10,11] In this model, dislocations located in the $\gamma$-$\gamma'$ interfaces act as sources of internal stresses. In the unloaded state, the hard $\gamma'$ phase remains in a forward and the soft $\gamma$ phase in a backward stressed state with respect to the applied stress. The residual deformation-induced internal strains in the directions [001] and [010], and $\varepsilon_{[001]}$ and $\varepsilon_{[010]}$, respectively, are evaluated from the deformation-induced changes in the lattice mismatch. Thus, the residual internal strain in the [001] direction is given by:

$$\varepsilon_{[001]} = \Delta(\delta)_{[001]} = \delta_{[001]} - \delta_{\text{undef}} \qquad [1]$$

For the strains in the [100] and/or [010] directions, analogous equations are valid. The difference between the internal stresses in the $\gamma$ and $\gamma'$ phases in the directions [001] and [010], $\Delta\sigma_{[001]}$ and $\Delta\sigma_{[010]}$, can be evaluated from the elastic deformation-induced internal strains in the $\gamma$ and $\gamma'$ phases via Hooke's generalized law, e.g., for $\Delta\sigma_{[001]}$, as:

$$\Delta\sigma_{[001]} = \frac{E}{(1+\nu)(1-2\nu)} \cdot \left[(1-\nu)\varepsilon_{[001]} + \nu\left(\varepsilon_{[100]} + \varepsilon_{[010]}\right)\right] \qquad [2]$$

where $\nu$ is Poisson's ratio. Note that this is a simplified approach that does not take into account that, for the continuous phase ($\gamma$ in cuboidal, $\gamma'$ in raft structure), different stress states exist in the regions aligned roughly parallel and perpendicular to the stress axis.[10] Stress equilibrium in the $\gamma$ and $\gamma'$ phases requires that the following relation holds between the local internal stresses $\Delta\sigma^{\gamma}$ and $\Delta\sigma^{\gamma'}$ (in a given direction) and the corresponding volume fractions $f^{\gamma}$ and $f^{\gamma'}$ of the $\gamma$ and $\gamma'$ phases, respectively:

$$\Delta\sigma^{\gamma} f^{\gamma} + \Delta\sigma^{\gamma'} f^{\gamma'} = 0 \qquad [3]$$

Although the Young's moduli of the $\gamma$ and $\gamma'$ phases are different, the present work uses the Young's moduli of the alloy for simplicity. To relate the internal stresses to the deformation process, it would be necessary to determine their value at the temperature of deformation by also taking into account the effect of thermally induced stresses. Because such data were lacking at the time of the authors' earlier report, thermally induced stresses were ignored in the previous publication.[12] In the interim, measurements of the line profiles were performed on unloaded specimens in the temperature range between room temperature and the temperatures of creep deformation.[15] Some important results of these measurements are summarized in the Appendix. These results indicate that the magnitudes of the internal stresses calculated from the data presented here for creep-deformed specimens that were unloaded and cooled to room temperature represent upper limits.

With this reservation, Eq 1 to 3 were used to obtain upper limits of the magnitudes of the internal stresses in the $\gamma$ and $\gamma'$ phases in the directions [001] and [010] for the appropriate temperatures. Use was made of the relevant high-temperature elastic data as follows: Young's modulus, $E$ (see Table 1); Poisson's ratio, $\nu = 0.395$, 0.398, and 0.407 for $T = 750$, 900, and 1050 °C, respectively.[16] The internal stresses are compressive in $\gamma$ along the [001] direction and in $\gamma'$ along the [010] direction and are tensile in $\gamma'$ along the [001] direction and in $\gamma$ along the [010] direction. In other words, forward internal stresses prevail in the hard $\gamma'$ phase, and internal back stresses prevail in the softer $\gamma$ phase. The largest internal stress prevails in $\gamma$ along the direction of the applied stress as follows: $\Delta\sigma^{\gamma}_{[001]} = -169$ and $-203$ MPa for $T = 900$ °C/$\sigma = 750$ MPa and 1050 °C/$\sigma = 305$ MPa, respectively. In the case of samples deformed at 750 °C, the internal stresses are different from those of the other samples; tension prevails in the directions [001] and [010] in $\gamma'$ and compression in both directions in $\gamma$. In the prerafted sample (sample 11) deformed at 750 °C, the internal stresses are larger than in the sample with the cuboidal $\gamma$-$\gamma'$ structure deformed at the same stress. This is in contrast to the results of samples deformed at 1050 °C with and without predeformation, which exhibit no differences.[11] In these latter samples, however, the microstructure at rupture is always raft-like.

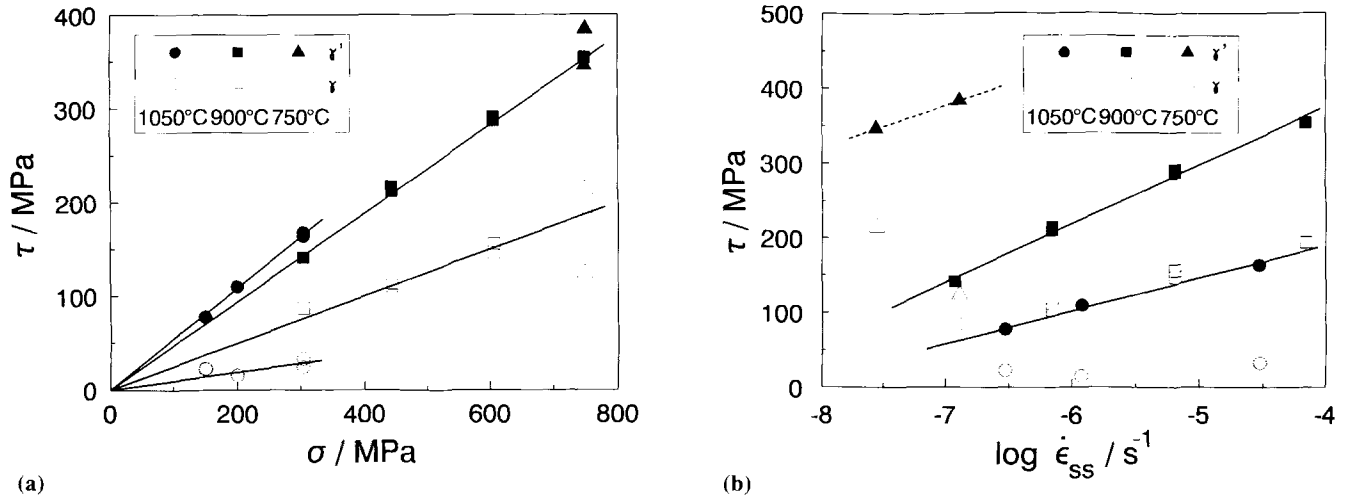


**Fig. 6** Local resolved shear stresses (a) in the phases γ and γ′ versus applied stress and (b) in the phase γ′ as a function of the quasistationary creep rate, $\dot{\epsilon}_{ss}$.

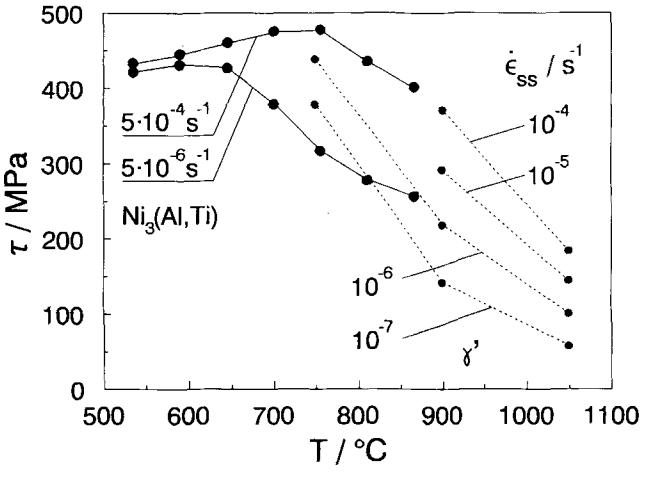


**Fig. 7** Critical resolved shear stress (in compression) of $Ni_3(Al,Ti)$ in the [001] direction for strain rates of $5 \times 10^{-6}$ s$^{-1}$ and $5 \times 10^{-4}$ s$^{-1}$, respectively,[18] and local shear stresses in the γ′ phase in stressed glide systems of the type {111}⟨101⟩.

The mismatch data of samples a and b through e, creep deformed at 900 °C at a stress of 305 MPa to different strains, show that the residual internal stresses develop after the minimum creep rate has been reached at a strain of 0.5%. During the subsequent deformation process, the internal stresses do not change significantly beyond 1.5% strain until rupture (sample e).

### 4.3 *Resolved Shear Stresses*

In the following, the procedure for calculating the overall resolved shear stresses acting in γ′ (and in γ) is described. Approximations will be used where exact quantitative values are not available. The overall resolved shear stress, τ, on the stressed slip systems of the type {111}⟨101⟩ due to the superposition of the external and internal stresses can be evaluated by the following relation for the stress in the γ′ phase, which is similar to an equation of Pollock and Argon:[17]

$$\tau^{\gamma}_{\{111\}\langle\bar{1}01\rangle} = \left(\sigma_{applied} + \Delta\sigma^{\gamma}_{[001]} - \Delta\sigma^{\gamma}_{[010]}\right)\frac{1}{\sqrt{6}} \qquad [4]$$

A similar relation holds for the stress in the γ phase. In this expression, the initial coherency stresses of the originally cuboidal γ′ particles are explicitly omitted, assuming that these coherency stresses correspond to a triaxial tensile stress state without shear stresses. At any rate, the internal stresses in the γ′ phase should be small, mainly due to the high volume fraction of γ′. Therefore, the evaluated resolved shear stresses in the γ′ phase are probably realistic approximations. In the case of the γ phase, Eq 4 should be interpreted in terms of the following contributions:[17] coherency stresses, orowan stresses, solid solution hardening, and dislocation-dislocation interactions, including hardening effects of gliding dislocations with dislocation networks situated at the γ-γ′-phase boundaries. Such a detailed evaluation is beyond the scope of this article.

Because the magnitudes of the internal stresses calculated previously represent upper bounds, the calculation of the overall resolved shear stresses, based on the use of these internal stresses in Eq 4, will lead to lower bound values for the γ phase and to upper bound values for the γ′ phase, respectively. This statement is correct for the data obtained at deformation temperatures of 900 and 1050 °C; it does not apply to samples deformed at 750 °C, in which the nature of the internal stresses was different (see Section 4.2). The values of the overall resolved shear stresses described above, i.e., $\tau^{\gamma}$ and $\tau^{\gamma'}$ acting in the phases γ and γ′, respectively, were determined as described above for all specimens investigated in this and in the authors' earlier study[11] and are plotted as a function of the applied stress in Fig. 6(a).

From the comparison of the values $\tau^{\gamma'}$ with the critical resolved shear stress (crss) of the γ′ phase at the appropriate temperature and strain rate, it should be possible to infer whether

the $\gamma'$ phase has yielded and has been penetrated by dislocations. For this purpose, the $\tau^{\gamma'}$ data (and the $\tau^{\gamma}$ data) are replotted in Fig. 6(b) as a function of the quasi-steady-state creep rate, $\dot{\varepsilon}_{ss}$ (at the beginning of the almost steady-state creep), which is taken as the relevant creep rate. From this plot, the locally acting shear stresses, $\tau^{\gamma'}$, are extracted for some given values of $\dot{\varepsilon}_{ss}$ and plotted as a function of temperature in Fig. 7. In this evaluation, the data of the prerafted specimen 11, which exhibited a higher subsequent creep rate,[13,14] were also used, because there were no other creep data at 750 °C available. The evaluated data are then compared with values from the literature with the crss values of $Ni_3(Al,Ti)$,[18] which corresponds approximately to the $\gamma'$ phase, as a function of temperature and for given strain rates. In view of the phenomenon of flow stress asymmetry, it must be pointed out, however, that the data in Ref 18 refer to compression tests. This comparison, although crude, shows that the $\tau^{\gamma'}$ values do indeed lie in the range of the crss values of $Ni_3(Al,Ti)$ reported for $\dot{\varepsilon} \approx 5 \times 10^{-6}\ s^{-1}$.

It should be noted that, in the earlier publication,[12] the range of creep rates, $\dot{\varepsilon}_{ss}$, for the $\gamma'$ phase was incorrectly stated as $10^{-8}$ to $10^{-5}\ s^{-1}$ instead of $10^{-7}$ to $10^{-4}\ s^{-1}$ in Fig. 7. This correction has, however, no consequences on the discussion of the figure. Figure 7 shows that the deformation of samples 10 and 11 at 750 °C falls within a range of strain rate and stress where the $\gamma'$ phase should be penetrated by dislocations. The shear stress in these samples is high enough to allow cutting, particularly because the shear stress is higher than that necessary for cutting of $Ni_3(Al,Ti)$ at a higher strain rate. This statement is supported by transmission electron microscopy (TEM) studies of these samples, which show cutting of $\gamma'$ with associated stacking faults.[19] At 900 °C, samples deformed at stresses of 607 and 750 MPa (samples 7, 8, and 9) also fall in that shear stress-temperature regime at the given strain rate, where cutting of $\gamma'$ seems to be possible. Besides the approximations mentioned previously, the current estimated data do not include the fact that the $\gamma$-$\gamma'$ phase boundaries are covered with dislocation networks, which has a hardening effect. They also ignore that $Ni_3(Al,Ti)$ is not identical to $\gamma'$ and do not take into account the presence of local stress concentrations in the microstructure, which could modify the actual local shear stresses.[17] This is particularly true in the cuboidal $\gamma$-$\gamma'$ microstructure. This factor, however, is more important for the $\gamma$ phase. Regarding the flow stress in the constrained $\gamma$ phase, factors such as, in particular, the absolute value of the coherency stresses in the initial state are not yet known reliably. Hence, as mentioned previously, a more detailed evaluation with respect to the different microstructural hardening contributions will not be attempted here.

## 5. Conclusions

- In the undeformed state, the monocrystalline alloy SRR 99 exhibits asymmetrical X-ray line profiles and has a negative lattice mismatch of $\delta_{undef} = -1.4 \times 10^{-3}$.
- In [001]-oriented samples creep deformed at stresses up to 750 MPa at different temperatures, the (002) and (020) line profiles are markedly different from each other. The asymmetry observed in the undeformed state is enlarged in the side case and *reversed* in the axial case.
- The change in the lattice mismatch was evaluated in terms of long-range internal stresses. The deformation-induced internal stresses are triaxial. They build up after the minimum creep rate and remain constant during quasi-steady-state creep until rupture.
- The internal stresses at room temperature of samples creep deformed till rupture at 900 and 1050 °C depend linearly on the applied stress.
- From the superposition of the triaxial internal stresses at the temperature of deformation and the applied external stress, the overall resolved shear stresses on the active glide systems were evaluated.
- The estimated resolved shear stresses acting in the $\gamma'$ phase were found to be comparable to the crss of $Ni_3(Al,Ti)$ for given strain rates.

### Acknowledgment

The authors are very grateful to Dr. J. Hammer for providing the samples, to Mr. M. Strehler for making available the results of the high-temperature measurements, and to Dr. R.R. Keller for a critical reading of the manuscript. The financial support of the Volkswagen-Stiftung is acknowledged gratefully (Az. I/65383).

## Appendix

### Summary of Measurements of X-Ray Line Profiles at High Temperatures

Measurements of the line profiles were performed in the unloaded state between room temperature and the temperatures of creep deformation, i.e., 750, 900, and 1050 °C.[15] The most important results can be summarized as follows.

As a general observation, it was noted that, during the high-temperature X-ray measurement, some recovery and relaxation of internal stresses occurred, as verified by subsequent repetition of room-temperature measurements. This effect became more pronounced the higher the temperature of deformation, and, hence, the higher were the largest temperatures at which the X-ray measurements were performed.

The following results are partly a consequence of this behavior.

X-ray line profiles of samples creep deformed at 1050 °C, measured at this deformation temperature, are almost identical for the side and axial cases. This result is a consequence of the fact that the misfit of the (002) line profiles, $\delta_{[001]}$, of the samples deformed at stresses of 150 and 305 MPa changes sign with increasing temperature and assumes almost the same value as $\delta_{[010]}$ ($\delta \approx -2.7 \pm 0.2 \times 10^{-3}$) at 1050 °C for both cases.

In the case of samples deformed at 750 and 900 °C, $\delta_{[010]}$ remains nearly constant over the entire temperature range. On the other hand, $\delta_{[001]}$ decreases for both temperatures above about 800 °C and approaches zero in the case of samples deformed at 900 °C.

From these high-temperature results, the following conclusion is relevant to the present work. Because of the possibility of recovery during measurement, the magnitudes of the internal stresses derived from the room-temperature measurements

are upper bounds for the internal stresses at the temperature of deformation. This justifies the manner in which the room-temperature data were used in the analysis of the internal stresses and the overall resolved shear stress in the present article (see Sections 4.2 and 4.3).

## References


1. D.D. Pearson, F.D. Lemkey, and B.H. Kear, Stress Coarsening of $\gamma'$ and Its Influence on Creep Properties of a Single Crystal Superalloy, *Superalloys 1980*, J.K. Tien, S.T. Wlodek, H. Morrow, M. Gell, and G.E. Maurer, Ed., American Society for Metals, 1980, p 513-520
2. R.A. MacKay and L.J. Ebert, The Development of $\gamma$-$\gamma'$ Lamellar Structures in a Nickel-Base Superalloy during Elevated Temperature Mechanical Testing, *Metall. Trans. A*, Vol 16, 1985, p 1969-1982
3. C. Carry and J.L. Strudel, Apparent and Effective Creep Parameters in Single Crystals of a Nickel Base Superalloy, Part II, *Acta Metall.*, Vol 26, 1978, p 859-870
4. P. Caron and T. Kahn, Improvement of Creep Strength in a Nickel-Base Single Crystal Superalloy by Heat Treatment, *Mater. Sci. Eng.*, Vol 61, 1983, p 173-184
5. M.V. Nathal, R.A. MacKay, and R.G. Garlick, Temperature Dependence of $\gamma$-$\gamma'$ Lattice Mismatch in Nickel-Base Superalloys, *Mater. Sci. Eng.*, Vol 75, 1985, p 195-205
6. A. Lasalmonie and J.L. Strudel, Interfacial Dislocation Networks around $\gamma'$ Precipitates in Nickel-Base Alloys, *Philos. Mag.*, Vol 32, 1975, p 937-949
7. R.C. Ecob, M.P. Shaw, A.J. Porter, and B. Ralph, The Application of Convergent-Beam Electron Diffraction to the Detection of Small Symmetry Changes Accompanying Phase Transformations, Part I, *Philos. Mag. A*, Vol 44, 1981, p 1117-1133
8. D. Bellet and P. Bastie, Temperature Dependence of the Lattice Parameter of the $\gamma$ and $\gamma'$ Phases in the Nickel-Based Superalloy CMSX-2. Part II: Neutron Diffraction Study of the Lattice Parameter Mismatch, *Philos. Mag. B*, Vol 64, 1991, p 143-152
9. L. Müller, T. Link, and M. Feller-Kniepmeier, Temperature Dependence of the Thermal Lattice Mismatch in a Single Crystal Nickel-Base Superalloy Measured by Neutron Diffraction, *Scr. Metall. Mater.*, Vol 26, 1992, p 1297-1302
10. H.-A. Kuhn, H. Biermann, T. Ungár, and H. Mughrabi, An X-Ray Study of Creep-Deformation Induced Changes of the Lattice Mismatch in the $\gamma'$-Hardened Monocrystalline Nickel-Base Superalloy SRR 99, *Acta Metall. Mater.*, Vol 39, 1991, p 2783-2794
11. H. Biermann, H.-A. Kuhn, T. Ungár, J. Hammer, and H. Mughrabi, Internal Stresses, Coherency Strains and Local Lattice Parameter Changes in a Creep-Deformed Monocrystalline Nickel-Base Superalloy, *Proc. 9th Int. Conf. Strength of Metals and Alloys*, Vol 1, D.G. Brandon, R. Chaim, and A. Rosen, Ed., Freund Publishing, London, 1991, p 421-428
12. H. Mughrabi, H. Biermann, and T. Ungár, X-Ray Analysis of Creep-Induced Local Lattice Parameter Changes in a Monocrystalline Nickel-Base Superalloy, *Superalloys 1992*, S.D. Antolovich, R.W. Stusrud, R.A. MacKay, D.L. Anton, T. Khan, R.D. Kissinger, and D.L. Klarstrom, Ed., The Minerals, Metals & Materials Society, 1992, p 599-608
13. J. Hammer, Kriech-und Zeitstandverhalten der einkristallinen Nickelbasis-Superlegierung SRR 99 unter besonderer Berücksichtigung der mikrostrukturellen Vorgänge und der Materialfehler (in German), Doctorate thesis, Universität Erlangen-Nürnberg, 1990
14. J. Hammer and H. Mughrabi, High-Temperature Creep and Microstructure of the Monocrystalline Nickel-Base Superalloy SRR 99, *Advanced Materials and Processes, Proc. First European Conf. Advanced Materials and Processes*, D. Driver and H. Mughrabi, Ed., DGM Informationsgesellschaft, Oberursel, 1990, p 445-600
15. M. Strehler, Bestimmung lokaler Gitterparameter und innerer Spannungen mittels Hochtemperatur-Röntgendiffraktometrie (in German), Diploma thesis, Universität Erlangen-Nürnberg, 1993
16. H.-A. Kuhn and H.G. Sockel, Contributions of the Different Phases of Two Nickel-Base Superalloys to the Elastic Behavior in a Wide Temperature Range, *Phys. Stat. Sol. (A)*, Vol 119, 1990, p 93-105
17. T.M. Pollock and A.S. Argon, Creep Resistance of CMSX-3 Nickel Base Superalloy Single Crystals, *Acta Metall. Mater.*, Vol 40, 1992, p 1-30
18. G.R. Leverant, M. Gell, and S.W. Hopkins, The Effect of Strain Rate on the Flow Stress and Dislocation Behavior of a Precipitation-Hardened Nickel-Base Alloy, *Mater. Sci. Eng.*, Vol 8, 1971, p 125-133
19. R.R. Keller, unpublished research, 1992